

# Late Breaking Results: Fast System Technology Co-Optimization Framework for Emerging Technology Based on Graph Neural Networks

Tianliang Ma<sup>†</sup>, Guangxi Fan<sup>†</sup>, Xuguang Sun, Zhihui Deng, Kainlu Low, Leilai Shao<sup>\*</sup>  
Shanghai Jiao Tong University, Shanghai, China

**Abstract**— This paper proposes a fast system technology co-optimization (STCO) framework that optimizes power, performance, and area (PPA) for next-generation IC design, addressing the challenges and opportunities presented by novel materials and device architectures. We focus on accelerating the technology level of STCO using AI techniques, by employing graph neural network (GNN)-based approaches for both TCAD simulation and cell library characterization, which are interconnected through a unified compact model, collectively achieving over a 100X speedup over traditional methods. These advancements enable comprehensive STCO iterations with runtime speedups ranging from 1.9X to 14.1X and supports both emerging and traditional technologies.

## I. INTRODUCTION

STCO integrates design and manufacturing early in chip development within the semiconductor industry, aiming to optimize performance, power efficiency, and yield through a unified consideration of design and manufacturing constraints. It enables concurrent exploration of materials, device structures, processes, and design choices, improving system performance and reliability. Nevertheless, the iterative nature of traditional STCO approaches prolongs development, necessitating innovative solutions to expedite the process [1].

Our work advances the acceleration of technology level tasks within the STCO domain, an area that attracts more attention in recent research. The tasks at this level often encounter significant challenges, such as time-intensive TCAD simulations for device optimization [2], the lack of standardized models in transistor modeling [3], and the complexities in cell library characterization with emerging technologies and process variations [4]. Fig. 1 outlines our primary contributions to address these challenges, incorporating a TCAD surrogate model and cell characterization model based on GNN techniques. Additionally, parameter extraction is facilitated through our unified compact model, validated across technologies such as carbon nanotube (CNT), indium gallium zinc oxide (IGZO), and low-temperature polycrystalline silicon (LTPS). Furthermore, the efficacy of our framework is validated by evaluating multiple designs using CNT technology, all conducted within the comprehensive STCO process depicted in Fig. 1.

## II. FAST SYSTEM TECHNOLOGY CO-OPTIMIZATION FRAMEWORK

The framework accelerates the traditional process by employing a reinforcement learning (RL) agent to explore the design space across diverse benchmarks based on CNT technology, including six ISCAS89 benchmarks, two AI accelerator MAC (multiplier accumulator) cores, and two open-sourced RISC-V cores. Our framework significantly enhances computational efficiency, reducing TCAD simulation time to 1.38 seconds and cell library characterization time to 8.88 seconds, beyond a shared environment setup time of 8.12 seconds for both processes. In contrast, commercial EDA tools require an average of 142.07 seconds for device simulations, as determined from a calibrated study involving 576 planar CNT devices with 2D TCAD simulations [5], and nearly 1900 seconds for cell library characterizations. These advancements demonstrate an acceleration exceeding 100 times for both individual tasks. For system evaluation, we utilized commercial tools for logic synthesis, placement & routing,

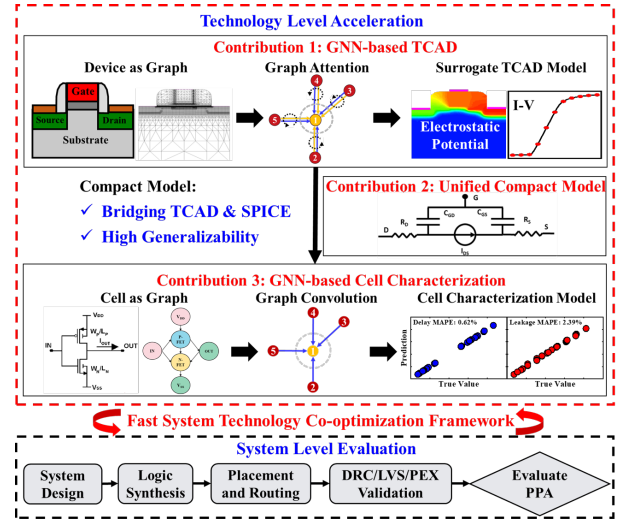


Fig. 1. Fast STCO framework based on GNN.

and DRC & LVS checks. As illustrated in Table I, the whole flow achieves a 1.9X to 14.1X acceleration over traditional flows per iteration. The framework focuses on technology acceleration, despite relying on commercial tools for system evaluation, promises notable speed gains. With numerous AI-driven methods available to hasten system evaluation, we anticipate even greater acceleration for our STCO framework ahead. In addition, though initially tested on CNT technology, its adaptability allows easy application to other technologies like IGZO and LTPS.

TABLE I  
RUNTIME COMPARISON BETWEEN FAST STCO TRADITIONAL FLOW

| Benchmarks | Approximate Runtime(s) |                            |      | Speedup(X) |
|------------|------------------------|----------------------------|------|------------|
|            | System Evaluation      | Traditional STCO Framework | Ours |            |
| s298       | 142                    | 2184                       | 160  | 13.6       |
| s386       | 136                    | 2178                       | 154  | 14.1       |
| s526       | 202                    | 2244                       | 220  | 10.2       |
| s820       | 198                    | 2240                       | 216  | 10.4       |
| s1196      | 223                    | 2265                       | 241  | 9.4        |
| s1488      | 230                    | 2272                       | 248  | 9.2        |
| 16bit MAC  | 536                    | 2578                       | 554  | 4.7        |
| 32bit MAC  | 1270                   | 3312                       | 1288 | 2.6        |
| Picorv32   | 939                    | 2981                       | 957  | 3.1        |
| Darkriscv  | 2250                   | 4292                       | 2268 | 1.9        |

Note: "Traditional STCO Framework" runtime combines system evaluation with commercial TCAD and cell library characterization times. "Ours" reflects system evaluation plus GNN-accelerated processes.

### A. GNN-based Surrogate Model for TCAD Simulation

The graph-based unified device encoding in Fig. 2 features material-level and device-level embeddings, alongside spatial relationship representation. Material-level embedding comprises a one-hot vector for material type delineation and a parameter vector that details material properties and parameterizes physical models, such as Shockley-Read-Hall (SRH) recombination and tunneling. Device-level embedding is designed to intricately characterize individual devices, utilizing a one-hot vector for regional traits and an attribute vector to specify the position and operational parameters, encompassing doping, bias, and more. Spatial relationship embedding, serving as edge features and inspired by finite element methods, represents the relative positions between nodes. In addition, the encoding enables inclusion of task-specific self-consistent features in device simulation like charge density, tailored to the different tasks.

Utilizing node and graph regression, we established a Poisson emulator and an IV predictor for device characterization respectively. The Poisson emulator integrated charge

<sup>†</sup>Tianliang Ma and Guangxi Fan contribute equally. <sup>\*</sup>Corresponding author: Leilai Shao (leilaishao@sjtu.edu.cn). This work was supported by the National Key Research and Development Program of China: Design Technology Co-Optimization Methodology (grant number: 2023YFB4402700).

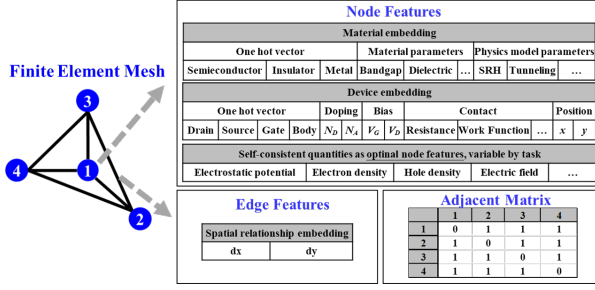


Fig. 2. Unified device encoding scheme based on finite element mesh details node and edge features with task-specific self-consistent quantities.

density as an additional feature, whereas the node features of the IV predictor included both charge density and potential. Architecturally, the Poisson emulator employed a deep graph attention network with edge feature (RelGAT) and comprised approximately 1 million parameters, incorporating a 12-layer GAT with 2 attention heads and one multilayer perceptron (MLP). In contrast, the IV predictor utilized a shallower RelGAT model with about 0.15 million parameters, featuring a 3-layer, single-head GAT with a 4-layer MLP for prediction. Layer normalization was applied in the training of both models, enhancing model convergence and stability across the dataset of 50,000 independent devices. Table II showcases the effectiveness of the RelGAT model, demonstrating its high accuracy through validation and testing. To further assess the generalizability, an additional test on 32,000 unseen data samples was conducted, indicating a highly accurate surrogate TCAD model.

TABLE II  
MSE OF SURROGATE TCAD IN THE WHOLE TESTING DATASET

|                  | Validation            | Testing               | Unseen(32K)           | $R^2(32K)$ |
|------------------|-----------------------|-----------------------|-----------------------|------------|
| Poisson Emulator | $6.17 \times 10^{-5}$ | $7.02 \times 10^{-5}$ | $7.15 \times 10^{-5}$ | 0.9999     |
| IV Predictor     | $1.67 \times 10^{-3}$ | $1.60 \times 10^{-3}$ | $1.78 \times 10^{-3}$ | 0.9999     |

### B. Unified Compact Model for Emerging Technologies

The compact model for emerging transistors is formulated to account for mobility variations in CNT, IGZO, and LTPS technologies due to charge drift in the presence of tail-distributed traps (TDTs) and variable range hopping (VRH) [3], as detailed in Eq. (1):

$$\mu = \begin{cases} \mu_0(V_G - V_{th})^\gamma, & \text{N-type TFT} \\ \mu_0(V_{th} - V_G)^\gamma, & \text{P-type TFT} \end{cases} \quad (1)$$

where  $V_{th}$  is the threshold voltage,  $\gamma$  is the field enhancement factor for mobility and  $\mu_0$  is defined as the effective mobility when  $|V_G - V_{th}| = 1$ . This model integrates mobility enhancement assumptions with the charge drift to develop an intrinsic current model. Validation against measured I-V curves from CNT, LTPS, and IGZO based devices is shown in Fig. 3.

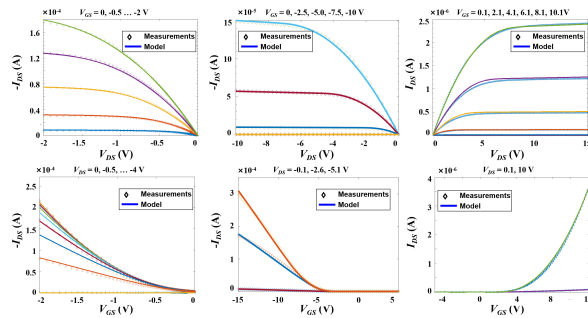


Fig. 3. Validations of the proposed TFT model with measured I-V curves: (a) CNT-TFT with  $L = 25\mu\text{m}$  and  $W = 125\mu\text{m}$ ; (b) LTPS-TFT with  $L = 16\mu\text{m}$  and  $W = 40\mu\text{m}$ ; (c) IGZO-TFT with  $L = 20\mu\text{m}$  and  $W = 30\mu\text{m}$ .

### C. GNN-based Fast Cell Library Characterization Model

Our methodology employs a two-stage process to advance cell characterization for semiconductor design. Initially, we developed a comprehensive cell library comprising 35 types

of combinational and sequential cells and utilized transistor-level SPICE simulation to generate extensive cell datasets for training and testing, encompassing nine metrics including delay, output slew, leakage power, capacitance (maximum capacitance of each input pin), flip power (dynamic power generated when both input and output pins are flipped), non-flip power (dynamic power generated when only the input pins are flipped, while the state of the output pin remains unchanged), minimum setup/hold time, and pulse width (for sequential cells only) under various corners and technology settings. In the second stage, we adopted a 3-layer graph convolutional network (GCN) to establish our framework. To enhance the accuracy of predictions, an additional 2-layer MLP was added after the GCN layers for each metric.

In our study of emerging technology, we utilized the unified compact model and specifically focused on analyzing the variation of supply voltage ( $V_{DD}$ ), threshold voltage ( $V_{th}$ ), and gate unit capacitance ( $C_{ox}$ ). These three critical parameters significantly influences the performance of emerging devices. The definitions of node features are presented in Table III. Here, "Current\_state" and "Next\_state" are two features related to the input pin state, with "1" denoting a high level and "0" representing a low level, respectively. "Input\_slew" denotes the transition time of input signal, "Output\_load" denotes capacitive load on cell output pins. For cell metrics that do not have relationship with some bits in the vector, these bits will be set to "0".

TABLE III  
NODE FEATURE VECTOR DEFINITION FOR SILICON TECHNOLOGY

|       | IN            | OUT         | N-FET                 | P-FET                 | $V_{DD}$ | $V_{SS}$ |
|-------|---------------|-------------|-----------------------|-----------------------|----------|----------|
| Bit0  | 0             | 0           | 0                     | 0                     | 1        | 1        |
| Bit1  | 0             | 1           | 1                     | 1                     | 0        | 0        |
| Bit2  | 1             | 0           | 1                     | 1                     | 0        | 1        |
| Bit3  | 0             | 0           | -1                    | 1                     | 0        | 0        |
| Bit4  | 0             | 0           | 0                     | 0                     | $V_{DD}$ | 0        |
| Bit5  | 0             | 0           | Width                 | Width                 | 0        | 0        |
| Bit6  | 0             | 0           | Gate Unit Capacitance | Gate Unit Capacitance | 0        | 0        |
| Bit7  | 0             | 0           | $V_{th}$              | $V_{th}$              | 0        | 0        |
| Bit8  | Input_slew    | 0           | 0                     | 0                     | 0        | 0        |
| Bit9  | 0             | Output_load | 0                     | 0                     | 0        | 0        |
| Bit10 | Current_state | 0           | 0                     | 0                     | 0        | 0        |
| Bit11 | Next_state    | 0           | 0                     | 0                     | 0        | 0        |

As detailed in Table IV, valid data from 125 corners were for training while from 512 corners for testing, the model demonstrated high accuracy in experiments. For flip power and non-flip power, the average error of prediction is relatively larger compared with other cell metrics, the reason is due to the fact that the dynamic power consumption varies by several orders of magnitude among different standard cells. The model exhibits a relatively large percentage error in predicting extremely low dynamic power consumption which needs to be improved in our future work.

TABLE IV  
MAPES OF CELL LIBRARY PREDICTION IN THE WHOLE TESTING DATASET

|                     | LTPS  | CNT   | Number of Data Points |
|---------------------|-------|-------|-----------------------|
| Delay               | 0.47% | 0.62% | 696320                |
| Output Slew         | 0.79% | 0.83% | 696320                |
| Capacitance         | 0.18% | 0.21% | 70656                 |
| Flip Power          | 5.74% | 4.96% | 696320                |
| Non-flip Power      | 3.36% | 5.60% | 393216                |
| Leakage Power       | 2.78% | 2.39% | 165888                |
| Minimum Pulse Width | 1.20% | 1.67% | 8192                  |
| Minimum Setup       | 0.50% | 0.27% | 16384                 |
| Minimum Hold        | 0.45% | 0.38% | 16384                 |

### REFERENCES

- [1] E. M. Bazizi et al., "Materials to Systems Co-Optimization Platform for Rapid Technology Development Targeting Future Generation CMOS Nodes," in IEEE Transactions on Electron Devices, vol. 68, no. 11, pp. 5358-5363, Nov. 2021, doi: 10.1109/LED.2021.3076757.
- [2] W. Jang et al., "TCAD Device Simulation With Graph Neural Network," in IEEE Electron Device Letters, vol. 44, no. 8, pp. 1368-1371, Aug. 2023, doi: 10.1109/LED.2023.3290930.
- [3] L. Shao et al., "Compact Modeling of Thin-Film Transistors for Flexible Hybrid IoT Design," in IEEE Design & Test, vol. 36, no. 4, pp. 6-14, Aug. 2019, doi: 10.1109/MDAT.2019.2899058.
- [4] F. Klemme, Y. Chauhan, J. Henkel and H. Amrouch, "Cell Library Characterization using Machine Learning for Design Technology Co-Optimization," 2020 IEEE/ACM International Conference On Computer Aided Design (ICCAD), San Diego, CA, USA, 2020, pp. 1-9.
- [5] L. Xu, C. Qiu, L. Peng, and Z. Zhang, "Suppression of leakage current in carbon nanotube field-effect transistors," Nano Res., vol. 14, no. 4, pp. 976-981, Apr. 2021, doi: 10.1007/s12274-020-3135-8.